J. Fluid Mech. (1983), *vol.* 126, *pp.* 147–165
Printed in Great Britain

Vortex shedding from a rectangular prism and a circular cylinder placed vertically in a turbulent boundary layer

By HIROSHI SAKAMOTO
Department of Mechanical Engineering, Kitami Institute of Technology, Kitami, 090, Japan

AND MIKIO ARIE
Hokkaido University, Sapporo, 060, Japan

(Received 22 September 1981 and in revised form 9 June 1982)

Measurements of the vortex-shedding frequency behind a vertical rectangular prism and a vertical circular cylinder attached to a plane wall are correlated with the characteristics of the smooth-wall turbulent boundary layer in which they are immersed. Experimental data were collected to investigate the effects of (i) the aspect ratio of these bodies and (ii) the boundary-layer characteristics on the vortex-shedding frequency. The Strouhal number for the rectangular prism and the circular cylinder, defined by $S = f_c w/U_0$ and $f_c d/U_0$ respectively, was found to be expressed by a power function of the aspect ratio h/w (or h/d). Here f_c is the vortex-shedding frequency, U_0 is the free-stream velocity, h is the height, w is the width and d is the diameter. As the aspect ratio is reduced, the type of vortex shedding behind each of the two bodies was found to change from the Karman-type vortex to the arch-type vortex at the aspect ratio of 2·0 for the rectangular prism and 2·5 for the circular cylinder.

1. Introduction

Wakes behind bluff bodies are so frequently encountered in engineering applications that researches have been conducted in large numbers and massive data accumulated. In particular, since von Kármán elucidated theoretically the vortex street formed behind a body, numerous reports have been published on theoretical and experimental aspects of the vortex street, including its formation mechanism (Nishioka & Sato 1978), stability (Taneda 1963), collapse (Taneda 1959), and effects of the wall on it Bearman & Zdravkovich 1978). Most of these studies are concerned, however, with uniform approaching flow. Meanwhile, the vortices formed behind a three-dimensional bluff body attached to a plane wall have such a complex nature that they pose difficult and interesting problems calling for further investigations.

In the neighbourhood of the base of a three-dimensional bluff body an adverse pressure gradient will be produced as a result of deflection of flow by an obstacle. Therefore a boundary layer will be forced to separate from the plane boundary wall and one or more vortices will be induced, being stretched around in the shape of a horseshoe. Then the flow will roll up into a number of continuously generated horseshoe-shaped vortices, wrapping up the base of the bluff body and trailing downstream subsequently in multiple vortex pairs with their axes parallel to the direction of the main flow. Thus these vortices will persist, moving with the stream, until they reach fairly far downstream. Furthermore, one main feature of the flow over the three-dimensional bluff body is its separation from the top and both of the side surfaces; thereby the separated flow is shed periodically downstream as an arch-type vortex.

Researches on the horseshoe vortex formed around the base of a bluff body attached to a plane wall have been carried out by several authors (e.g. Furuya & Miyata 1972; Norman 1975; Castro & Robins 1977; Hunt *et al.* 1978). A fairly recent study was reported by Baker (1979). He investigated experimentally the horseshoe vortex formed around the base of a cylinder by a separating laminar boundary layer, and found that both steady and unsteady vortex systems exist.

On the other hand, experimental investigations on Strouhal numbers and the system of the vortex shed behind a bluff body attached to a plane wall have also been reported by several authors. Through their measurements of Strouhal numbers obtained by changing the aspect ratio of a circular cylinder of finite height which is placed on a plane wall, Okamoto & Yagita (1973) made it clear that the Strouhal numbers vary with spanwise positions of the cylinder. From measurements of Strouhal numbers of a rectangular prism and a circular cylinder of finite height that is placed on a plane wall, Vickery (1968) reported that the Strouhal number decreases with decreasing aspect ratio in both cases. Meanwhile, Mochizuki (1961) investigated experimentally, using a visualization technique, the wake flow behind a sphere of various diameters on a plane in a laminar boundary layer, whereby she demonstrated that the wake begins to be deformed periodically and a characteristic row of the arch-type vortex is formed. In particular, Okamoto, Yagita & Kataoka (1977) observed the arch-type vortex behind a cone on a plane wall and suggested that the vortex changes from the arch type to the Kármán type with changing geometrical size of the cone.

However, a systematic investigation aimed at clarifying a relationship between variation of the geometrical size of a body and the type of vortices shed behind it has not been performed yet. The present study concerned itself principally with the Strouhal number of vortices shed behind a three-dimensional bluff body and elucidates experimentally differences existing in Strouhal number and type of vortices shed behind a body in a turbulent boundary layer in terms of the aspect ratio, using a prism of a square cross-section and circular cylinder, which are considered to represent the typical shapes of three-dimensional bodies attached to the plane wall.

2. Parameters to be included

The governing parameters in describing the Strouhal number of the rectangular prism and circular cylinder attached to a plane wall on which a turbulent boundary layer exists will now be considered. Since the bodies are immersed in a turbulent boundary layer as shown in figure 1, the characteristics of the boundary layer must first be specified.

As one of the simplest cases of turbulent boundary layers, one considers a fully developed boundary layer with zero pressure gradient along a smooth flat plate aligned with the main flow. The characteristics of the boundary layer such as the thickness δ, the surface shear stress τ_0, the shape factor H are functions of the Reynolds number $R_{\bar{X}} = U_0\bar{X}/\nu$, where $\bar{X}$ is the longitudinal distance measured from an appropriate virtual origin of the boundary layer. In practical cases, however, the determination of the origin for $\bar{X}$ is usually rather difficult. Therefore it may be more reasonable in practice to describe the characteristics of the boundary layer in terms of the local values of boundary-layer thickness, the surface shear stress and so on at the position where the test bluff body will be located rather than in terms of the Reynolds number. Hence the boundary-layer velocity distribution that would be measured at the location of the bluff bodies if they were absent is taken as the reference profile in the present work.

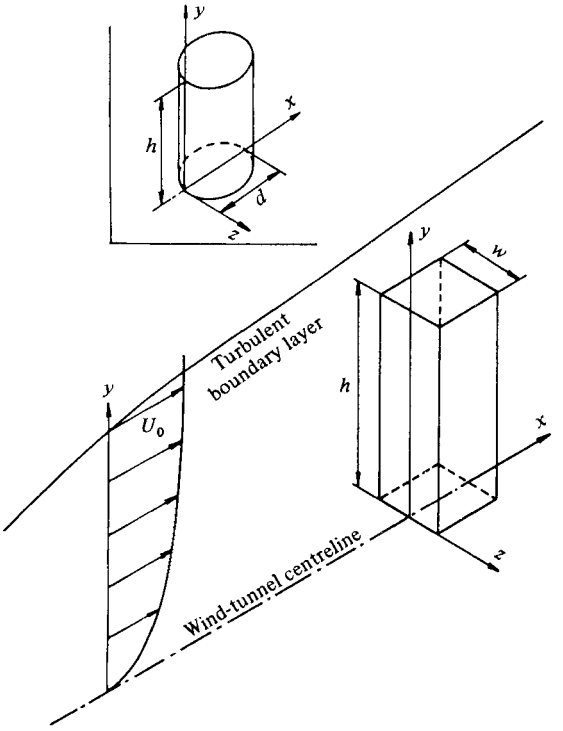

FIGURE 1. Coordinate system and definition sketch.

According to Coles (1956), the longitudinal velocity component in the equilibrium turbulent boundary layer can be expressed as

$$\frac{u}{u_\tau} = \frac{1}{\kappa}\ln\frac{yu_\tau}{\nu} + C + \frac{\Pi}{\kappa}w\left(\frac{y}{\delta}\right), \tag{1}$$

where κ and C are universal constants, w is a universal function of y/δ usually called the wake function, and Π is a profile parameter. Since $u = U_0$ at the position of $y = \delta$, (1) may be written as

$$\frac{U_0}{u_\tau} = \frac{1}{\kappa}\ln\frac{\delta u_\tau}{\nu} + C + \frac{\Pi}{\kappa}w(1). \tag{2}$$

Accordingly, from (2), the equilibrium turbulent boundary layer of this type can be described in terms of four parameters: the free-stream velocity U_0, the boundary-layer thickness δ, the friction velocity u_τ and the kinematic viscosity ν. The variables characterizing the geometrical shape of the two bodies dealt with in the present paper are determined as follows: the height h and the width w in the case of the rectangular prism, and the height h and diameter d of the circular cylinder.

Therefore the functional relationship for the frequency f_c of vortex shedding from the prism and the cylinder placed vertically in a turbulent boundary layer can be written as

$$f_c = f(h, u_\tau, U_0, \mu, \rho, h, w \text{ or } d). \tag{3}$$

By dimensional analysis, one gets the following functional relationships from (3):

$$S = \frac{f_c w}{U_0}\left(= \frac{f_c d}{U_0}\right) = f_1\left(\frac{u_\tau}{U_0}, \frac{h}{\delta}, \frac{hU_0}{\nu}, \frac{h}{w} \text{ or } \frac{h}{d}\right). \tag{4}$$

Since three parameters u_τ/U_0, h/δ and hU_0/ν included in the right-hand side of (4) are connected with one another by (2), two of them can be changed independently. Accordingly, the functional relationship of (4) can finally be put in the form

$$S = f_2\left(\frac{u_\tau}{U_0}, \frac{h}{\delta}, \frac{h}{w} \text{ or } \frac{h}{d}\right). \tag{5}$$

Consequently, the main purpose of the present investigation is to clarify the functional relationship of (5) by varying the above sets of three non-dimensional parameters.

3. Experimental equipment and procedure

3.1. *Wind tunnel*

The experimental work was carried out in two closed-circuit wind tunnels installed at the Kitami Institute of Technology. All the measurements for the Strouhal number were undertaken in a wind tunnel with a uniform test section 0·4 m high, 0·4 m wide and 4 m long. A series of four turbulence-reducing screens are installed in the settling section upstream of the contraction channel (contraction ratio 14:1), and the free-stream turbulence level in the test section is about 0·2% at the maximum free-stream velocity of 20 m/s that was employed in the present experiment. The ceiling of the test section of the tunnel is made of a flexible sheet of stainless steel so that its shape can be adjusted to remove the longitudinal pressure gradient. Also, the floor of the test section of the wind tunnel consists of a smooth plastic plate of thickness 10 mm, except for a steel plate 460 mm wide on which a test body was mounted, in order to eliminate the effect of the roughness of the surface, because the floor itself is used as the plane boundary along with the turbulent boundary layer develops.

Vortices formed behind a body were observed by the smoke-wire method in a closed-circuit wind tunnel, which had a uniform test section, 180 mm × 180 mm in cross-section and 2 m in length. A test body was placed on an acrylic plate 3 mm in thickness, which was put horizontally in the measurement portion, with the distance of 40 mm between the upper surfaces of the plate and the floor.

3.2. *Visualizing apparatus*

A visualizing apparatus using the smoke-wire method (see Torii 1977) consists of a discharge circuit (applying the current to a smoke wire), a delay circuit, a stroboscope (illuminating smoke streams) and a camera (photographing them). A smoke wire 0·2 mm in diameter is made of Nichrome; given sufficient tension, it is fixed onto a probe made of a stainless-steel pipe 6 mm in diameter. The oil was a mixture of liquid paraffin and kerosene, which was painted uniformly on the Nichrome wire with a fine writing brush.

3.3. *Test bodies*

Prepared for the present experiment were several rectangular prisms, each with a square cross-section, and circular cylinders. The heights selected for measuring vortex-shedding frequency behind the prism were 25, 37, 50, 60, 70 and 83·5 mm, and the aspect ratio h/w was varied in a range between 0·5 and 8·0. The heights of the cylinder were 21, 33, 45, 58, 74 and 88 mm, and the aspect ratio h/d was varied in a range between 1·0 and 8·0. Prism widths and cylinder diameters were selected for each aspect ratio of the prism and cylinder. Also, the prisms of five different aspect

ratios (h/w = 1, 2, 3, 4 and 5) with various heights (h = 15–132 mm) were prepared in order to examine an effect of the parameter h/δ on the Strouhal number. Further, for flow visualization in the wake of the prism and cylinder the heights of the bodies selected ranged from those approximately buried in the boundary layer to those protruding slightly from it.

3.4. *Detection of the vortex shedding*

For measuring the frequency of vortices shed behind a body a probe of a constant-temperature hot-wire anemometer was placed at a position (x/w = 2·0, y/h = 0·6, z/w = 0·6–1·0) for prisms and a position (x/d = 2·0, y/h = 0·5, z/d = 0·6–0·7) for cylinders. The hot-wire signal was recorded on a data recorder. The data were later processed by a data-acquisition and analysis system (Kyowa Dengyo Co.: DAAS-500A).

3.5. *Characteristics of the turbulent boundary layer*

The turbulent boundary layer developing along the smooth floor of the test section was employed in the present investigation. In this subsection it will be ascertained whether a fully developed equilibrium turbulent boundary layer was established or not at the location of the test body.

The mean-velocity profile in the boundary layer agreed well with the data of Kelbanoff & Diehl (1952). The mean-velocity profile in the region near the wall was confirmed to follow the logarithmic law suggested by Coles (1956):

$$\frac{u}{u_\tau} = 5{\cdot}75 \log \frac{yu_\tau}{\nu} + 5{\cdot}1. \tag{6}$$

The distribution of the longitudinal turbulence intensity in the boundary layer at the location of the test body agreed well with Klebanoff & Diehl's (1952) data.

The two-dimensionality of the flow in the boundary layer was examined by measuring velocity profiles at several positions in the direction normal to a free stream. The results showed that a satisfactory two-dimensionality at the location of the test body was realized in the region of 200 mm, which included the centreline of the test section. Further, the flexible ceiling of the wind tunnel was so adjusted as to yield zero-pressure gradient in the streamwise direction. Since the maximum deviation of pressure from the mean value was within $\pm 0{\cdot}1$ % of the dynamic pressure of the free stream, it may be judged that the condition of zero pressure gradient has been satisfactorily realized.

From the above, it would be concluded that the turbulent boundary layer employed in the present investigation had the same characteristics as a fully developed equilibrium turbulent boundary layer along a smooth plane wall under zero pressure gradient.

The characteristics of the undisturbed boundary layers at the location of the test body are summarized in table 1. The tripping rod of diameter d_0 included in this table was attached at the entrance of the test section in order to change the characteristics of the boundary layer. Also, the turbulent boundary layer with thickness δ = 30 mm was prepared particularly to examine the Strouhal number of the prisms with five aspect ratios (see figure 11) when h/δ are large.

The flow visualization around the prisms and the circular cylinders was performed by the smoke-wire technique at a fixed free-stream velocity U_0 = 0·7 m/s in the wind channel. In this observation, the boundary layer was laminar and its thickness was about 20 mm at the location of the test body.

Run			1	2	3
Free-stream velocity	U_0	(m/s)	10	15	20
Tripping rod	d_0	(mm)	6	6	6
Boundary-layer thickness	δ	(mm)	58·0	59·5	59·2
Displacement thickness	δ^*	(mm)	8·73	8·15	8·10
Momentum thickness	θ	(mm)	6·50	6·13	6·12
Shear velocity	u_τ	(m/s)	0·393	0·570	0·746
Shape factor	H		1·34	1·33	1·32
Reynolds number	R_θ		4128	5906	7332

TABLE 1. Characteristics of the undisturbed turbulent boundary layer at the location of prisms and cylinders

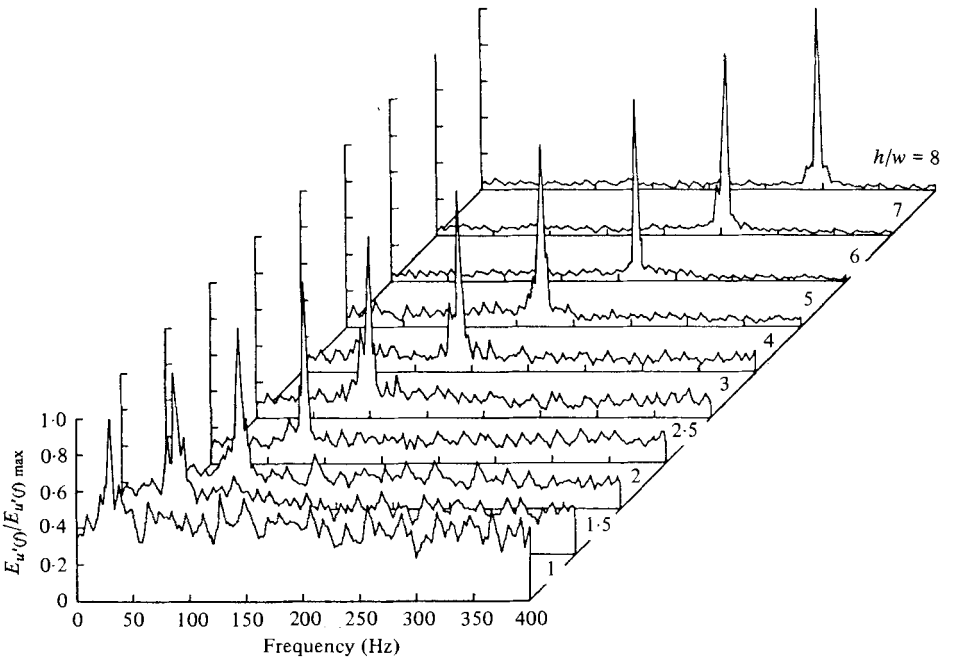

FIGURE 2. An example of vortex-shedding frequency and power spectrum of fluctuating velocity downstream of prisms of height 37 mm ($h/\delta = 0{\cdot}62$) and aspect ratios 1–8.

4. Presentation and discussion of results

Shown in figure 2 is the power spectrum $E_{u'(f)}$ of the fluctuating velocity u' downstream of prisms of height 37 mm ($h/\delta = 0{\cdot}62$) placed in a boundary layer shown as run 2 in table 1. In the figure the ordinate respresents the value of the power spectrum $E_{u'(f)}$, the value being non-dimensionalized using the maximum power spectrum $E_{u'(f)\,\max}$, whereas the abscissa represents frequency f(Hz). As is obvious from the figure, a prominent prevailing frequency f_c is observed behind each of the prisms over the aspect-ratio range from 1 to 8; it is suggested that vortices with this prominent f_c are shed behind the prism. In a range of h/w less than 1·0, however, no prominent f_c is found for the rectangular prisms adopted in the present experiment. Moreover, it is shown in this figure that, with decreasing h/w, the difference between the peak spectrum at the prominent f_c and the magnitude of the spectra at other frequencies becomes smaller gradually, and, accordingly, it is then likely that the strength of the vortex shedding from the prism decreases.

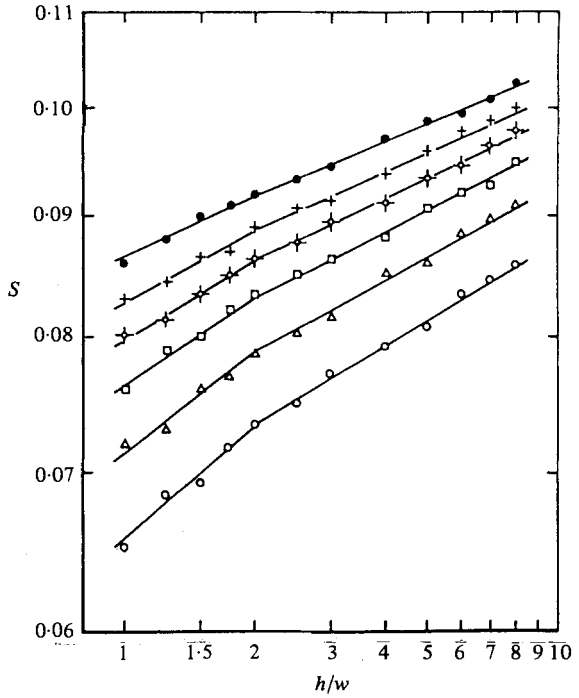

FIGURE 3. Strouhal number versus aspect ratio h/w for prisms of various heights in the Reynolds-number range (defined as $U_0 w/\nu$) $3{\cdot}06 \times 10^3$–$8{\cdot}2 \times 10^4$: ○, $h/\delta = 0{\cdot}42$; △, 0·62; □, 0·84; ⊹, 1·01; +, 1·18; ●, 1·40.

Shown in figure 3 is a relationship between the aspect ratios of rectangular prisms, with a range of heights and widths, and the Strouhal number S, which is defined by

$$S = \frac{f_c w}{U_0}. \tag{7}$$

The parameter u_τ/U_0 has a constant value for all data included in figure 3. Each line that has a nodal point in the vicinity of $h/w = 2{\cdot}0$ shown in figure 3 is the best-fit line obtained by the least-squares method. Most of the data were included within the $\pm 3\%$ region around each line. The same degree of accuracy was also obtained for all the other Strouhal numbers that were measured in this study. As is obvious from figure 3, with increasing h/w we notice an increase in S for all rectangular prisms. Moreover, S may be expressed as a power function of h/w for each value of h/δ. It is worth noting that in the vicinity of $h/w = 2{\cdot}0$ a different behaviour of S is observed with regard to h/w. It appears that this difference results from a change in shed vortices behind the prism, as will become obvious from the flow visualization to be discussed later. From the abovementioned result, S for a rectangular prism can be written as

$$S = C_1\left(\frac{h}{w}\right)^{n_1} \quad \left(1{\cdot}0 \leqslant \frac{h}{w} \leqslant 2{\cdot}0\right), \tag{8a}$$

$$S = C_2\left(\frac{h}{w}\right)^{n_2} \quad \left(\frac{h}{w} > 2{\cdot}0\right), \tag{8b}$$

where the coefficients C_1, C_2, n_1 and n_2 are functions of h/δ alone, and are given in figure 4.

The smoke patterns in the wake of the rectangular prisms are presented in figures

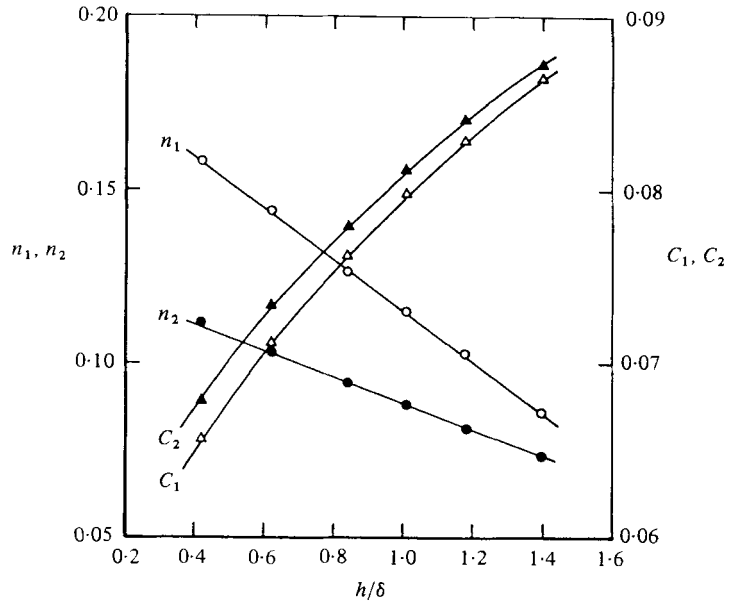

FIGURE 4. Relation between coefficients C_1, C_2, n_1, n_2 and h/δ: △, C_1; ▲, C_2; ○, n_1; ●, n_2.

5(*a*, *b*). In all the flow patterns, a smoke wire was set horizontally at the position (0·5–0·7)h above the floor of the tunnel. Although the boundary layer was laminar when visualizations were made, the qualitative nature of the wake flow patterns is assumed to be unchanged. Vortices formed behind a rectangular prism are classified into two major types: the first is the so-called Kármán vortex street in which a pair of vortices are arranged asymmetrically; the second is the so-called arch-type vortex in which a pair of vortices are arranged symmetrically as shown in figure 6. As is obvious from the figure, for prisms of h/w not larger than about 2·0, the wake vortices belong to the second type, and for those of $h/w > 2{\cdot}0$ the vortices belong to the first type. This change of vortex patterns is reflected by a change in the variation of Strouhal number in the vicinity of $h/w = 2{\cdot}0$ (see figure 3). Alternate formation of the first and the second type of vortices was observed in the vicinity of $h/w = 2{\cdot}0$. The probable reason for this change is that, when the side of a rectangular prism is relatively larger than the width of the prism, the flows separating from both sides are so much stronger than the flow from the top that the wake behind the prism is almost controlled by the flows from the sides. Consequently, the flows separating from both sides form the Kármán-type vortex street. With an increase in the width of the prism, the flow separating from the top end of the prism increases in strength; as a result, the flow from the top end joins the flows from the sides, forming an entity in the arch-type vortex, and is shed behind the prism. Moreover, when the vortices are of the second type, the width of the wake is much smaller than in the case of the first type. Accordingly, it is conjectured that the velocity fluctuation caused by the shedding of the second type becomes smaller than that in the first type. Consequently, when vortices change from the first type to the second type, the level of fluctuating velocity caused by the vortex shedding approaches the level of other irregular fluctuating velocities; thus the prominent prevailing frequencies are no longer detectable in the range smaller than $h/w = 1{\cdot}0$.

Figure 7 shows $S = f_c d/U_0$ for circular cylinders, with a range of heights and diameters, plotted against the aspect ratio h/d. Measurements were made by keeping

u_τ/U_0 constant, since it was made obvious that in the case of the rectangular prism this parameter has little effect on S, as mentioned below. It is observed from this figure that for a cylinder of any height, values of S are distributed on each line that has a kink in the vicinity of $h/d = 2{\cdot}5$, which is believed to come from the change of wake vortices from the arch-type vortex to the Kármán-type vortex, as was seen in the case of the rectangular prism. Moreover, regardless of the height, it was not possible to detect the prominent prevailing frequency f_c for $h/d < 1{\cdot}5$.

The foregoing result and figure 7 lead to the following empirical equations, which give S for a circular cylinder of finite height in a range of $h/d \leqslant 8{\cdot}0$ in the form

$$S = C_3\left(\frac{h}{d}\right)^{n_3} \quad \left(1{\cdot}5 \leqslant \frac{h}{d} \leqslant 2{\cdot}5\right), \tag{9a}$$

$$S = C_4\left(\frac{h}{d}\right)^{n_4} \quad \left(\frac{h}{d} > 2{\cdot}5\right), \tag{9b}$$

where the coefficients C_3, C_4, n_3, n_4 are functions of h/δ alone, and are given in figure 8.

Next, figures 9(a, b) show the result of the flow visualization. As is obvious from the figure, the vortex is observed to change from the arch-type vortex to the Kármán-type vortex in the vicinity of $h/d = 2{\cdot}5$; it is understood that this change corresponds to the change in the Strouhal number shown in figure 6. Moreover, it is observed in this vicinity that the two types of vortices are formed intermittently.

Figure 10 shows the distribution of the correlation coefficient $R_{u'u'}$ of the longitudinal velocity fluctuations in the shear layers separated from the sides of rectangular prisms of height $h = 70$ mm ($h/\delta = 1{\cdot}18$). For h/w larger than 2·0 there exists a negative value of the correlation, which indicates that the phase differs by almost half a period on both sides of the prism. For h/w less than 2·0, however, $R_{u'u'}$ approaches zero rapidly; this feature is believed to result from the change of wake vortices into arch-type vortices.

Shown next in figure 11 is the result of a study using five different aspect ratios ($h/w = 1$, 2, 3, 4 and 5) of the prism with various heights ($h = 15$–132 mm). In this plot, the effect of the parameter h/δ on the Strouhal number S is made clearer. It is observed that for all the aspect ratios, values of S collapse onto each line, and that they have an approximately constant value of 0·106 when h/δ exceed about 3·0. Figure 12 shows a comparison of S for a prism having a sufficiently large height compared with the thickness of a boundary layer. The data obtained by Vickery (1968), Kamei (1976), and by this experiment in a range $h/\delta > 3{\cdot}0$ are also included in this figure. Values of S are approximately constant in a range $S = 0{\cdot}100$–$0{\cdot}108$ in the cases studied by Vickery ($h/w < 5$) and Kamei ($h/w < 8{\cdot}0$). Accordingly, it is concluded that S is not subject to the influence of the boundary layer existing on the floor in the range $h/\delta > 3{\cdot}0$.

Figure 13 shows the distributions of the Strouhal number S at different spanwise positions y/h for four different aspect ratios ($h/w = 1{\cdot}5$, 3, 5 and 8). The Strouhal numbers are constant over almost the whole span in each case. This agrees well with Kamei's result, in which S along the height of the prism is constant for h/w up to 8·0.

From the description so far, it is clear that, when u_τ/U_0 has a constant value, S for the prism depends on two parameters h/w and h/δ contained in (5). Examined next is an effect of another remaining parameter u_τ/U_0 on S. Three different values of this parameter (runs 1, 2 and 3 in table 1), are tested for the prism with $h/w = 5$.

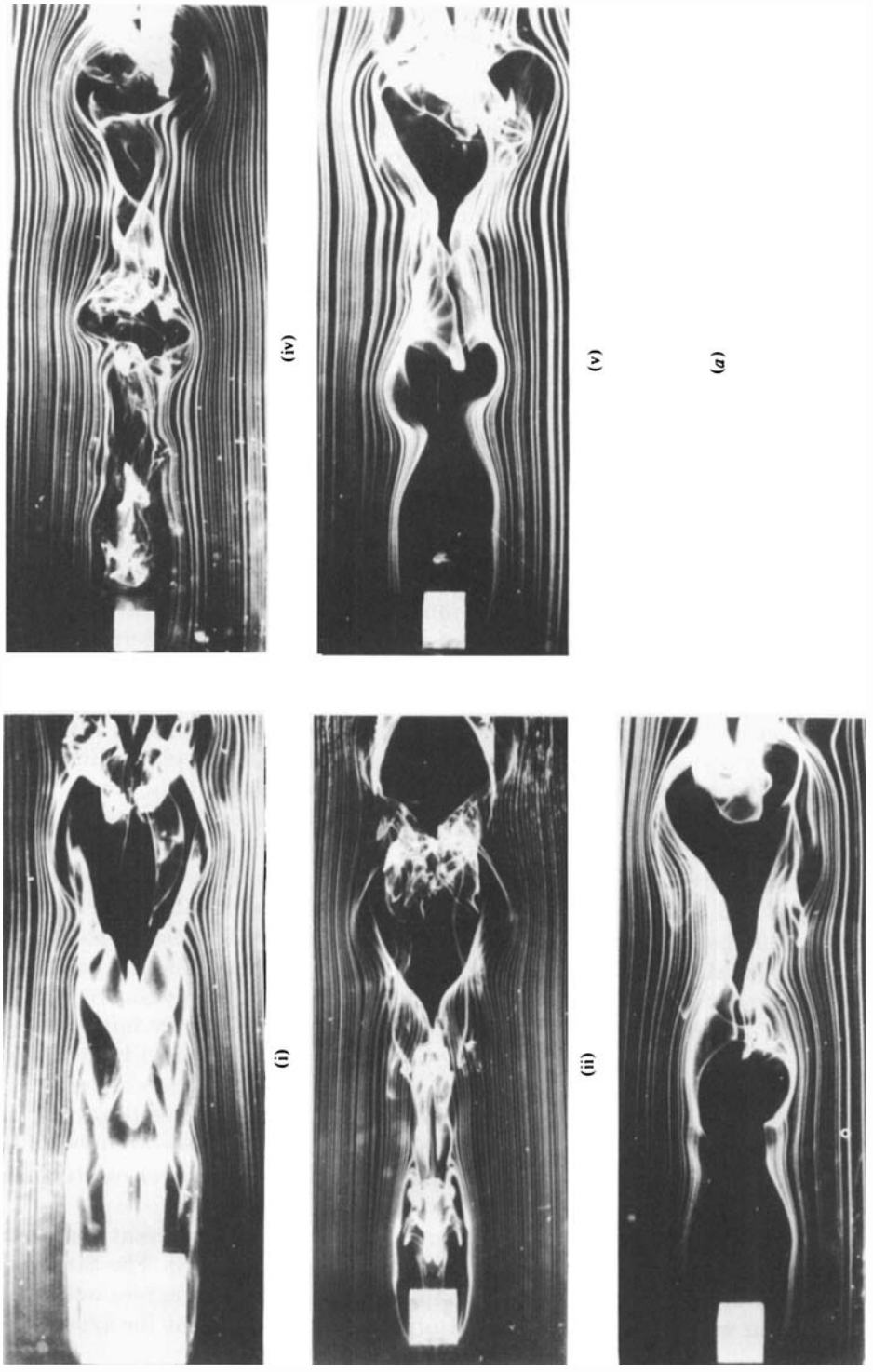

FIGURE 5. For caption see facing page.

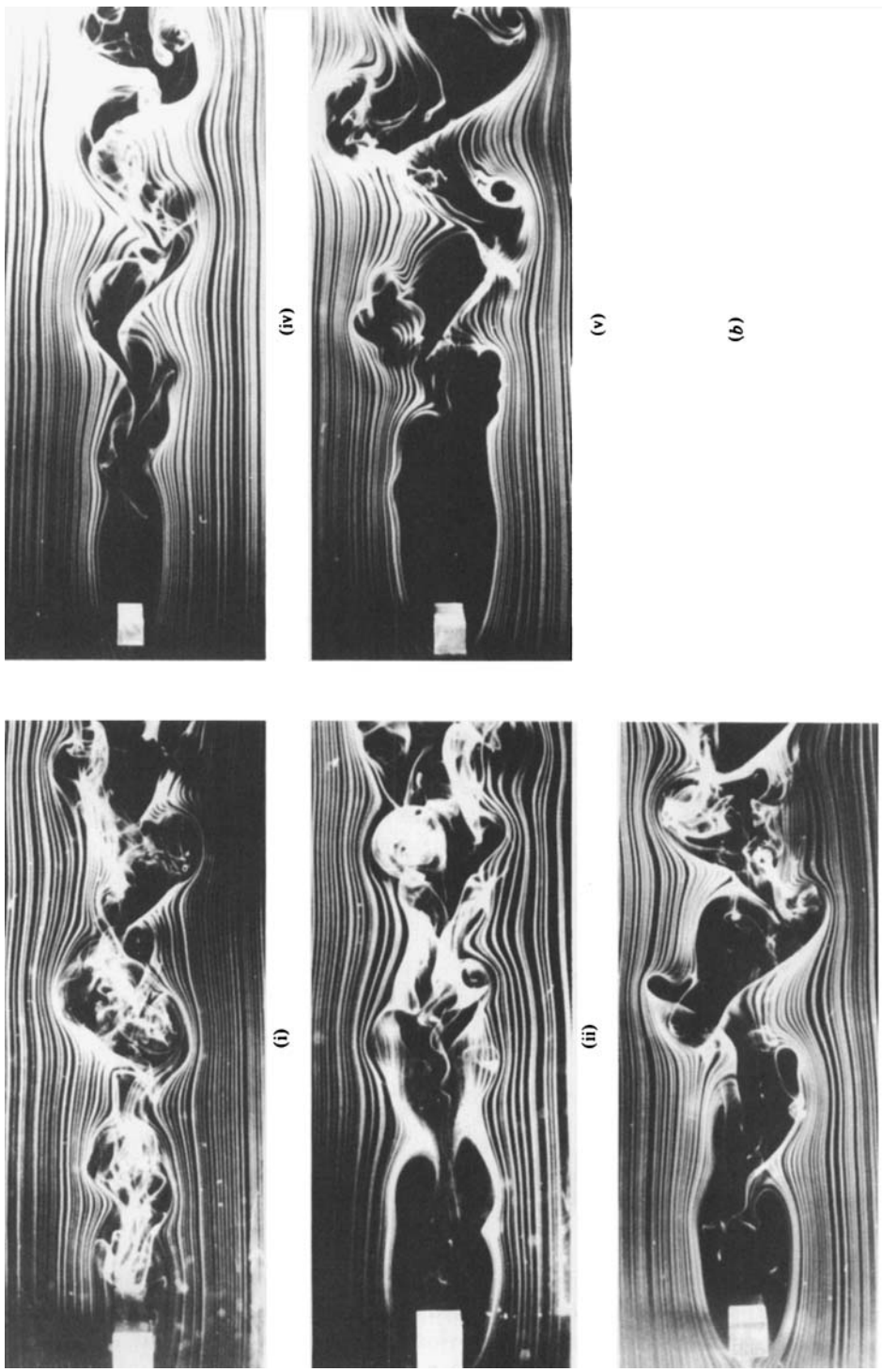

FIGURE 5. The smoke patterns in the wake of prisms of $h/\delta = 0{\cdot}8$–$1{\cdot}5$ in the Reynolds-number range (defined as $U_0 w/\nu$) $2{\cdot}7 \times 10^2$–$7{\cdot}3 \times 10^2$. (*a*) The wake vortices are arch-type vortices: (i) $h/w = 0{\cdot}5$; (ii) 1·0; (iii) 1·5; (iv) 1·75; (v) 2·0. (*b*) The wake vortices are Kármán-type vortices: (i) $h/w = 1{\cdot}75$; (ii) 2·0; (iii) 3·0; (iv) 4·0; (v) 5·0.

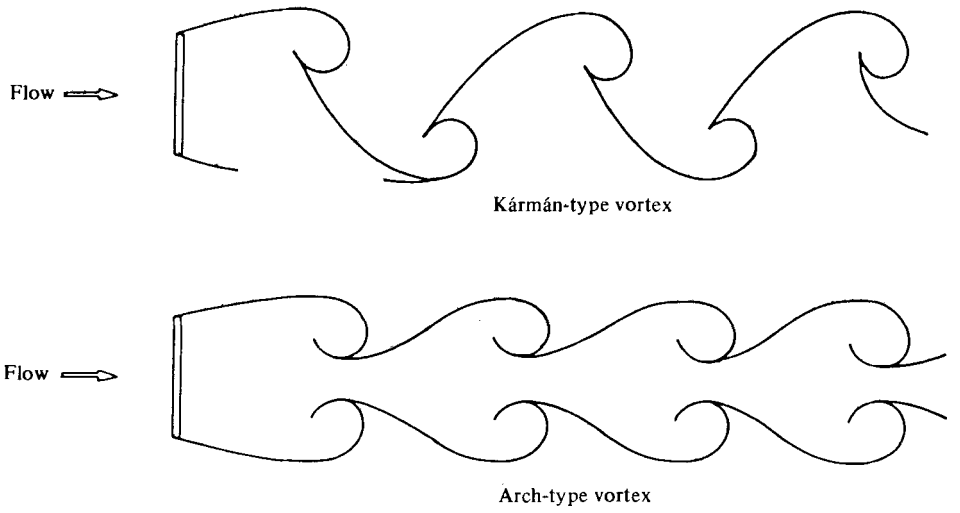

FIGURE 6. Sketch of two types of vortex formed behind the prism.

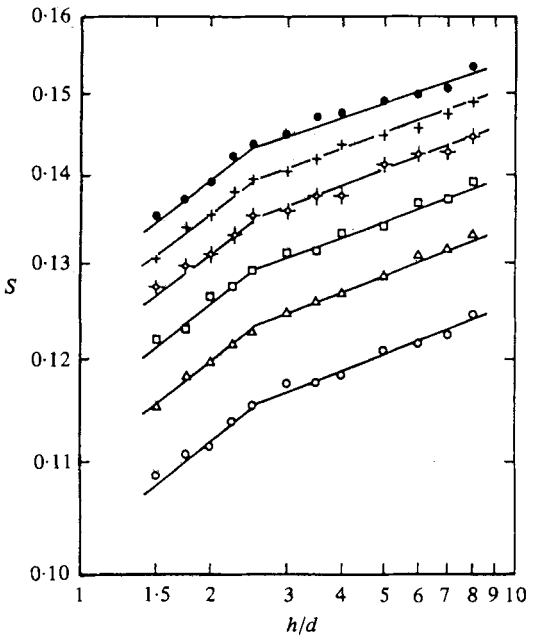

FIGURE 7. Strouhal number versus aspect ratio h/d for cylinders of various heights in the Reynolds-number range (defined as $U_0 d/\nu$) $2{\cdot}6 \times 10^3$–$5{\cdot}7 \times 10^4$: ○, $h/\delta = 0{\cdot}35$; △, 0·56; □, 0·76; ⊹, 0·98; +, 1·24; ●, 1·48.

Figure 14 shows the result of this examination. It is obvious that its effect on S is not prominent and that the data collapse onto a single line regardless of the values of u_τ/U_0. It follows then that among the three parameters contained in (5) the parameter u_τ/U_0 is considered to have only a slight effect, while h/w and h/δ have almost dominating effects. Note that u_τ/U_0 changes only slightly in this experiment; thus it will become necessary to investigate the effect of u_τ/U_0 over a wide range on S in the future study.

The foregoing results show that, given the aspect ratio and the thickness δ of a

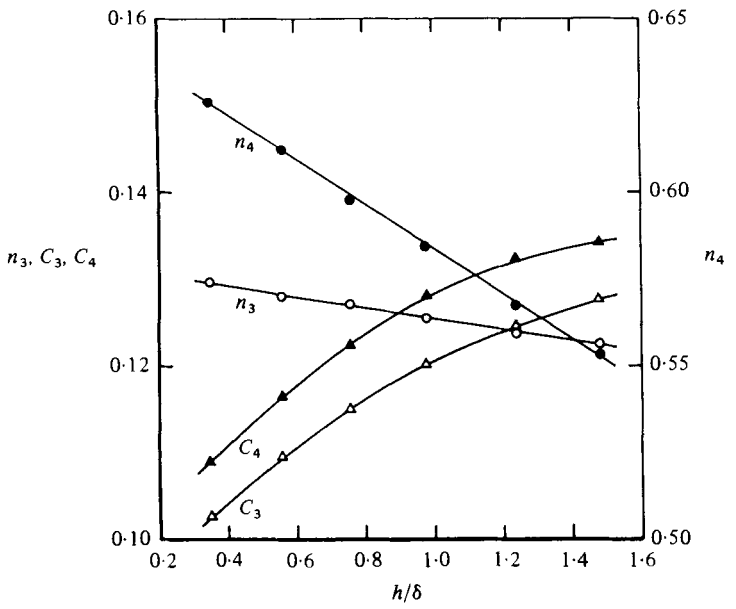

FIGURE 8. Relation between coefficients C_3, C_4, n_3, n_4 and h/δ: △, C_3; ▲, C_4; ○, n_3; ●, n_4.

turbulent boundary layer at the location in which the prism or circular cylinder of finite height is to be placed vertically in a turbulent boundary layer, then the Strouhal number S can be obtained from (8) and (9).

5. Concluding remarks

The present paper has described experimentally the vortex shedding from prismatical bars of rectangular and circular cross-sections of finite height, which are attached to a plane wall, with a turbulent boundary layer developing along the wall.

Two types of vortex are formed behind the body, depending on the aspect ratio; they are the arch-type vortex and the Kármán-type vortex. The former appears at an aspect ratio less than 2·0 and 2·5 for rectangular and circular cylinders, respectively, whereas the latter appears for the aspect ratio greater than the above values. This change of the wake vortices is reflected by a change in the variation of Strouhal number with aspect ratio. An empirical relation is obtained to estimate the Strouhal number in terms of the body shape and the boundary-layer characteristics.

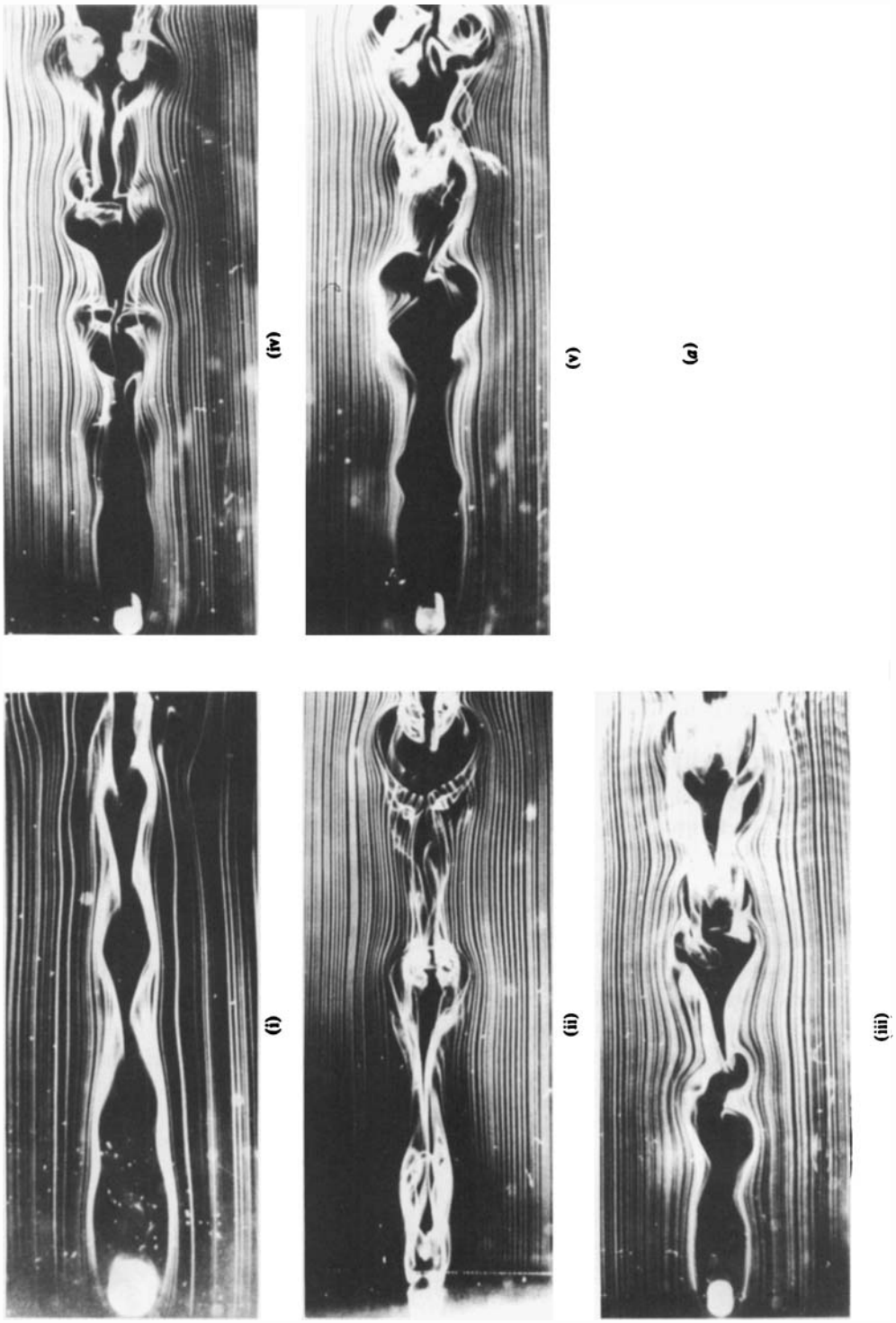

FIGURE 9. For caption see facing page.

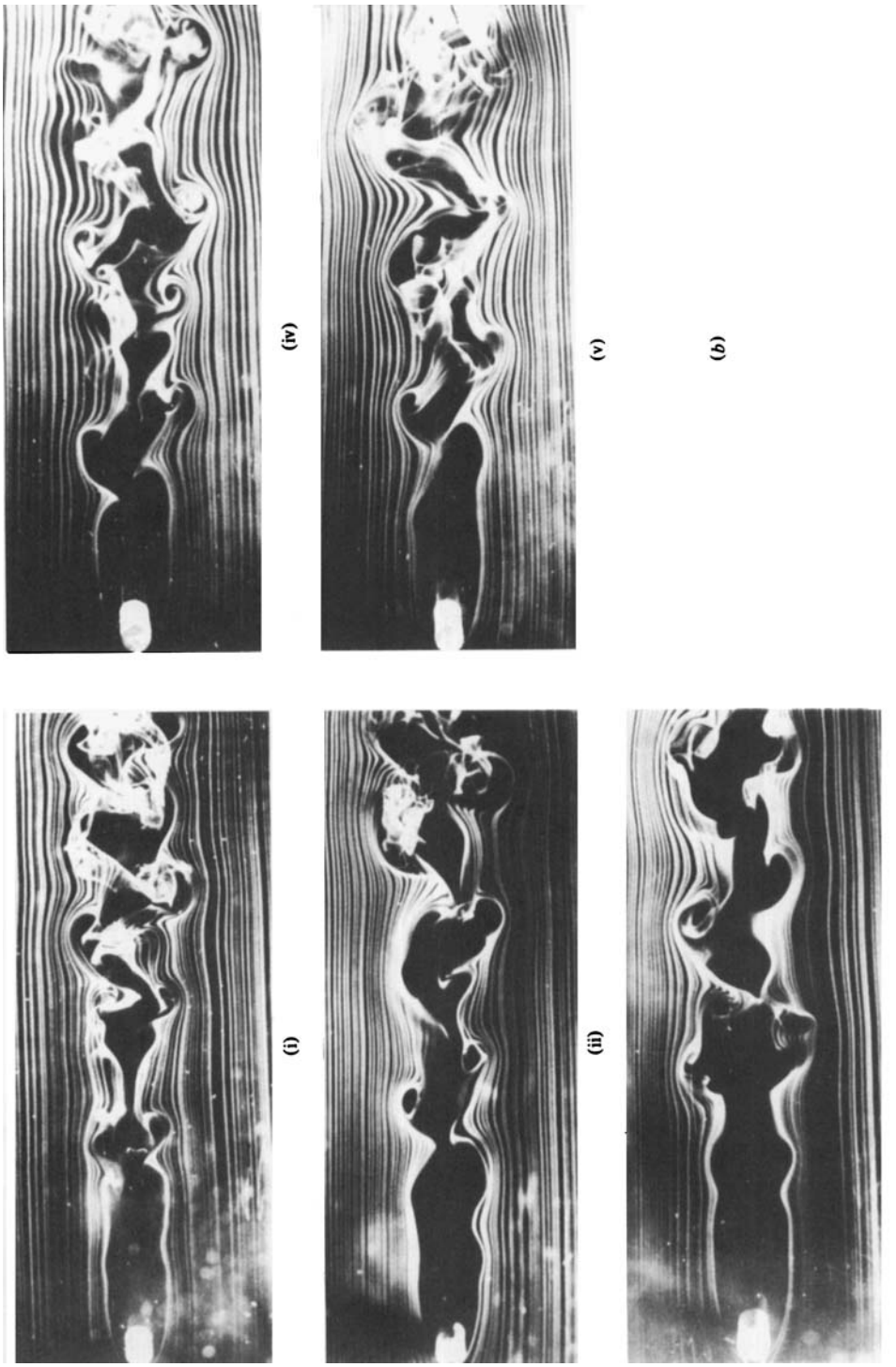

FIGURE 9. *The smoke patterns in the wake of cylinders of* $h/\delta = 1{\cdot}0 \sim 1{\cdot}5$ *in the Reynolds-number range (defined as* $U_0 d/\nu$*)* $2{\cdot}7 \times 10^2$–$9{\cdot}2 \times 10^2$. (*a*). The wake vortices are arch-type vortices: (i) $h/d = 1{\cdot}0$; (ii) 1·5; (iii) 2·0; (iv) 2·5; (v) 2·75. (*b*). The wake vortices are Kármán-type vortices: (i) $h/d = 2{\cdot}5$; (ii) 2·75; (iii) 3·0; (iv) 4·0; (v) 5·0.

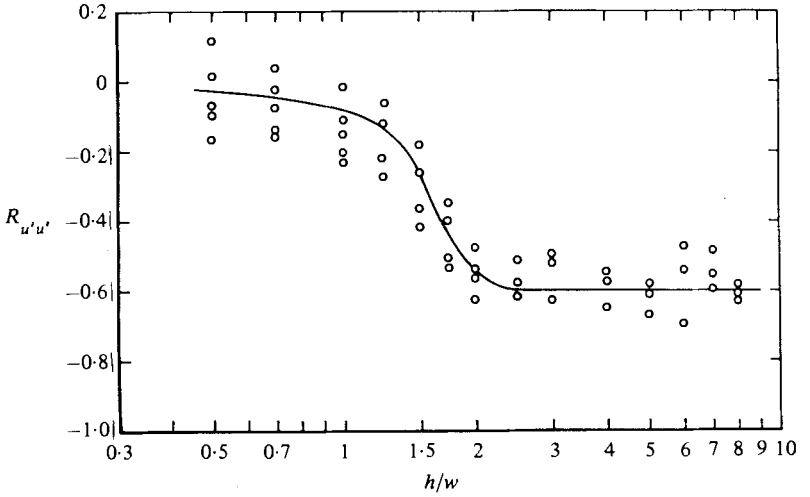

FIGURE 10. Variation of correlation measured at the sides of prisms of height 70 mm ($h/\delta = 1{\cdot}18$) with aspect ratio h/w.

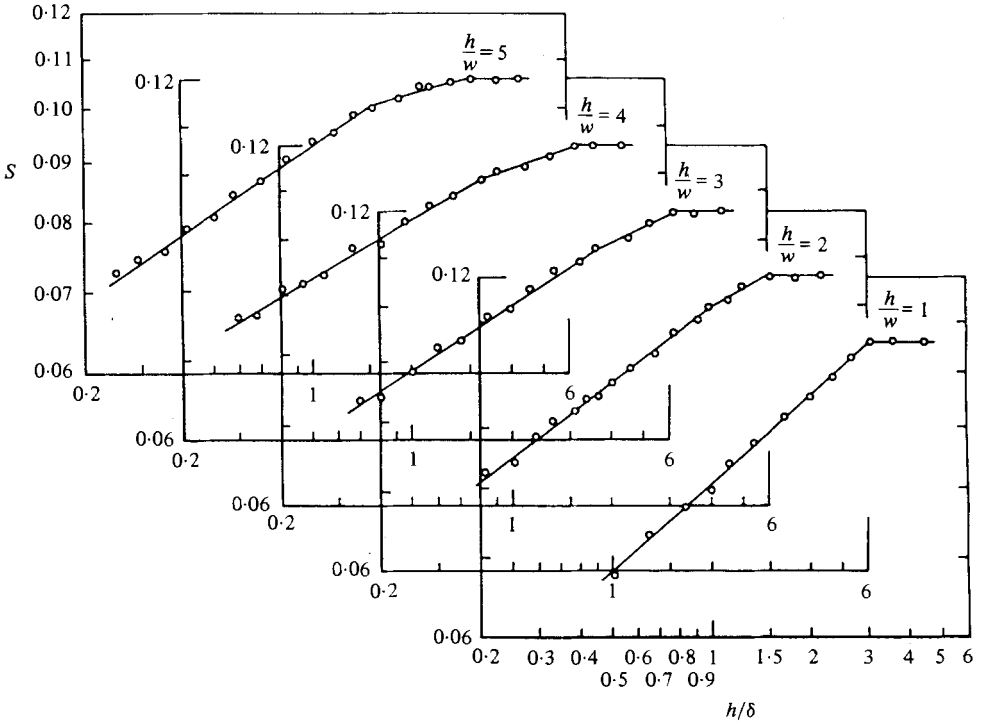

FIGURE 11. Strouhal number versus parameter h/δ for prisms of aspect ratios 1–5.

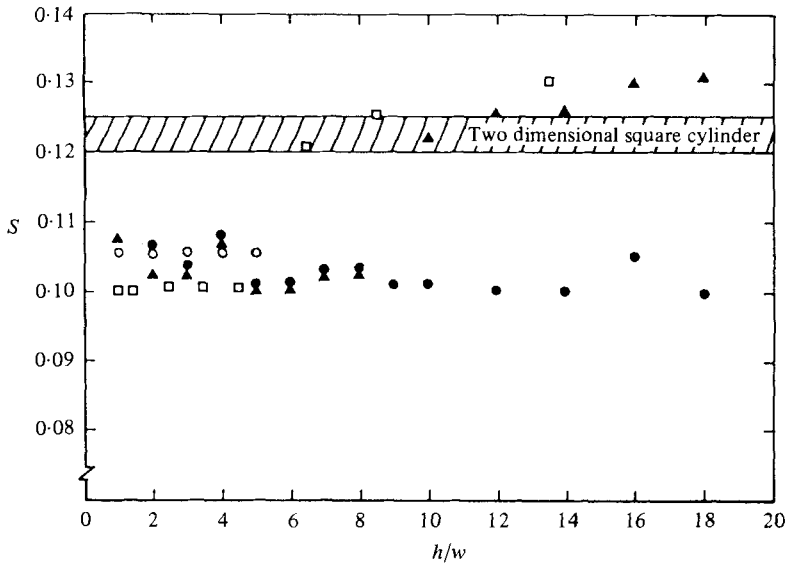

FIGURE 12. Strouhal number versus aspect ratio h/w for prisms at large h/δ: ○, present results ($h/\delta > 3{\cdot}0$); ▲, Kamei (1976) $y/h = 0{\cdot}50$; ○, Kamei $y/h = 0{\cdot}75$; □, Vickery (1968).

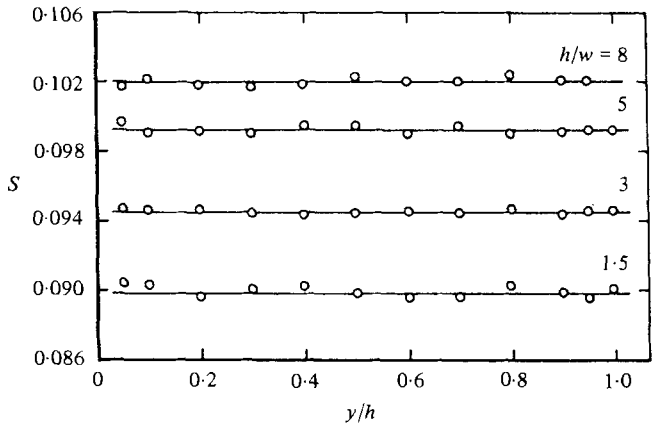

FIGURE 13. Transition of Strouhal number with spanwise position y/h for prisms of height 83·5 mm ($h/\delta = 1{\cdot}40$) and aspect ratios 1·5–8.

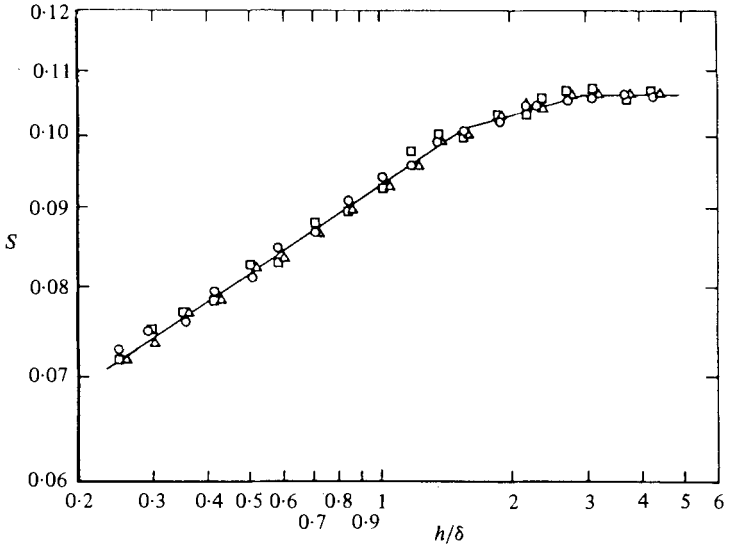

FIGURE 14. Strouhal number versus parameter u_τ/U_0 for prisms of aspect ratio 5: △, $u_\tau/U_0 = 0{\cdot}0393$; ○, 0·0380; □, 0·0373.

The authors express their sincere thanks to Dr M. Kiya for interesting discussions on the experimental results and also to Mr M. Moriya and Mr Y. Obata for their assistance in the construction of the experimental apparatus.

REFERENCES

BAKER, C. J. 1979 The laminar horseshoe vortex. *J. Fluid Mech.* **95**, 347.

BEARMAN, P. W. & ZDRAVKOVICH, M. M. 1978 Flow around a circular cylinder near a plane boundary. *J. Fluid Mech.* **89**, 33.

CASTRO, I. & ROBINS, A. 1977 The flow around a surface-mounted cube in uniform and turbulent streams. *J. Fluid Mech.* **79**, 307.

COLES, D. 1956 The law of the wake in the turbulent boundary layer. *J. Fluid Mech.* **1**, 191.

FURUYA, Y. & MIYATA, M. 1972 Visual studies on the wake of a roughness element proximate to a wall. *Mem. Fac. Engng, Nagoya Univ.* **24**, 278.

HUNT, J. C. R., ABELL, C. J., PETERKA, J. A. & WOO, H. 1978 Kinematical studies of the flows around free or surface-mounted obstacles; applying topology to flow visualization. *J. Fluid Mech.* **86**, 179.

KAMEI, E. 1976 Vortex shedding from a long cylinder of square cross section (in Japanese). *Preprint of JSAE* no. 2168, 771.

KLEBANOFF, P. S. & DIEHL, Z. W. 1952 Some features of artifically thickened fully developed turbulent boundary layer with zero pressure gradient. *NACA Tech. Rep.* no. 1110.

MOCHIZUKI, M. 1961 Smoke observations on boundary layer transition caused by a spherical roughness element. *J. Phys. Soc. Japan* **16**, 995.

NISHIOKA, M. & SATO, H. 1978 Mechanism and determination of the shedding frequency of vortices behind a cylinder at lower Reynolds numbers. *J. Fluid Mech.* **89**, 49.

NORMAN, R. S. 1975 Visualization of local fields using scale models. In *Proc. 2nd U.S. Nat. Conf. Wind Engng Res. Fort Collins*, p. iv-3-1.

OKAMOTO, T. & YAGITA, M. 1973 The experimental investigation on the flow past a circular cylinder of finite length placed normal to the plane surface in a uniform stream. *Bull. J.S.M.E.* **16**, 805.

OKAMOTO, M., YAGITA, M. & KATAOKA, S. 1977 Flow past cone on flat plate. *Bull. J.S.M.E.* **20**, 329.

TANEDA, S. 1959 Downstream development of the wakes behind cylinders. *J. Phys. Soc. Japan* **14**, 843.

TANEDA, S. 1963 The stability of two-dimensional laminar wakes at low Reynolds number. *J. Phys. Soc. Japan* **18**, 288.

TORII, K. 1977 Flow visualization by smoke-wire technique. In *Proc. Int. Symp. Flow Visualization, Tokyo*, p. 175.

VICKERY, B. J. 1968 Load fluctuations in turbulent flow. *Proc. A.S.C.E.: J. Engng Mech. Div.* **1**, 31.